Efficiency enhancement of screen-printed multicrystalline silicon solar cells by integrating gold nanoparticles via a dip coating process

Narges Fahim,[1] Zi Ouyang,[1] Yinan Zhang,[1] Baohua Jia,[1,3] Zhengrong Shi,[2] and Min Gu[1,4]

[1]*Centre for Micro-Photonics, Faculty of Engineering and Industrial Sciences, Swinburne University of Technology, PO Box 218, Hawthorn, 3122 Victoria, Australia*

[2]*Suntech Power Holdings Co., Ltd., 9 Xinhua Road, New District, Wuxi, Jiangsu Province 214028, China*

[3]*bjia@swin.edu.au*

[4]*mgu@swin.edu.au*

Abstract: Multicrystalline silicon solar cells play an increasingly important role in the world photovoltaic market. Boosting the comparatively low energy conversion efficiency of multicrystalline silicon solar cells is of great academic and industrial significance. In this paper, Au nanoparticles of an optimized size, synthesized by the iterative seeding method, were integrated onto industrially available surface-textured multicrystalline silicon solar cells via a dip coating method. Enhanced performance of the light absorption, the external quantum efficiency and the energy conversion efficiency were consistently demonstrated, resulting from the light scattering by the sized-tailored Au nanoparticles placed on the front surface of the solar cells, particularly in the spectral range from 800 to 1200 nm, an enhancement of the external quantum efficiency by more than 11% near λ = 1150 nm and the short-circuit current by 0.93% were both observed. As a result, an increase in the energy conversion efficiency up to 1.97% under the standard testing conditions (25°C, global air mass 1.5 spectrum, 1000 Wm^{-2}) was achieved. This study opens new perspectives for plasmonic nanoparticle applications for photon management in multicrystalline silicon solar cells.

OCIS codes: (040.5350) Photovoltaic; (250.5403) Plasmonics; (310.6628) Subwavelength structures, nanostructures; (310.3915) Metallic, opaque, and absorbing coatings; (160.4236) Nanomaterials.

References and links

1. M. Schmela, "PV in the fast lane: market survey on world cell production in 2000," Photon. Int. **3**, 32–35 (2001).
2. A. G. Aberle, P. P. Altermatt, G. Heiser, S. J. Robinson, A. Wang, J. Zhao, U. Krumbein, and M. A. Green, "Limiting loss mechanisms in 23% efficient silicon solar cells," J. Appl. Phys. **77**(7), 3491–3504 (1995).
3. T. L. Temple and D. M. Bagnall, "Optical properties of gold and aluminium nanoparticles for silicon solar cell applications," J. Appl. Phys. **109**(8), 084343 (2011).
4. D. M. Schaadt, B. Feng, and E. T. Yu, "Enhanced semiconductor optical absorption via surface plasmon excitation in metal nanoparticles," Appl. Phys. Lett. **86**(6), 063106 (2005).
5. B. P. Rand, P. Peumans, and S. R. Forrest, "Long-range absorption enhancement in organic tandem thin-film solar cells containing silver nanoclusters," J. Appl. Phys. **96**(12), 7519–7526 (2004).
6. S. Pillai, K. R. Catchpole, T. Trupke, and M. A. Green, "Surface plasmon enhanced silicon solar cells," J. Appl. Phys. **101**(9), 093105 (2007).
7. P. Matheu, S. H. Lim, D. Derkacs, C. McPheeters, and E. T. Yu, "Metal and dielectric nanoparticle scattering for improved optical absorption in photovoltaic devices," Appl. Phys. Lett. **93**(11), 113108 (2008).
8. Y. Tanaka, H. Hachimura, T. Mishima, and M. Ihara, "Plasmon effect in Si solar cells coated with a thin polymer film containing silver or Au nanoparticles," ECS Trans. **33**, 81–91 (2011).

#160131 - $15.00 USD Received 16 Dec 2011; revised 13 Jan 2012; accepted 13 Jan 2012; published 20 Jan 2012

9. S. H. Lim, W. Mar, P. Matheu, D. Derkacs, and E. T. Yu, "Photocurrent spectroscopy of optical absorption enhancement in silicon photodiodes via scattering from surface plasmon polaritons in gold nanoparticles," J. Appl. Phys. **101**(10), 104309 (2007).
10. S. P. Sundararajan, N. K. Grady, N. Mirin, and N. J. Halas, "Nanoparticle-induced enhancement and suppression of photocurrent in a silicon photodiode," Nano Lett. **8**(2), 624–630 (2008).
11. F. J. Beck, S. Mokkapati, and K. R. Catchpole, "Plasmonic light-trapping for Si solar cells using self-assembled Ag nanoparticles," Prog. Photovolt. Res. Appl. **18**(7), 500–504 (2010).
12. T. L. Temple, G. D. K. Mahanama, H. S. Reehal, and D. M. Bagnall, "Influence of localized surface plasmon excitation in silver nanoparticles on the performance of silicon solar cells," Sol. Energy Mater. Sol. Cells **93**(11), 1978–1985 (2009).
13. G. Frens, "Controlled nucleation for the regulation of the particle size in monodisperse gold suspensions," Nat. Phys. Sci (Lond.) **241**, 20–22 (1973).
14. K. R. Brown, D. G. Walter, and M. J. Natan, "Seeding of colloidal Au nanoparticle solutions. 2. Improved control of particles size and shape," Chem. Mater. **12**(2), 306–313 (2000).
15. S. Link and M. A. El-Sayed, "Size and temperature dependence of the plasmon absorption of colloidal Au nanoparticles," J. Phys. Chem. B **103**(21), 4212–4217 (1999).
16. J. Rodríguez-Fernández, J. Pérez-Juste, F. J. García de Abajo, and L. M. Liz-Marzán, "Seeded growth of submicron Au colloids with quadrupole plasmon resonance modes," Langmuir **22**(16), 7007–7010 (2006).
17. H. R. Stuart and D. G. Hall, "Absorption enhancement in silicon-on-insulator waveguides using metal island films," Appl. Phys. Lett. **69**(16), 2327–2329 (1996).
18. K. L. Kelly, E. Coronado, L. Zhao, and G. Schatz, "The optical properties of metal nanoparticles: the influence of size, shape, and dielectric environment," J. Phys. Chem. B **107**(3), 668–677 (2003).
19. S. Pillai, K. R. Catchpole, T. Trupke, T. Zhang, J. Zhao, and M. A. Green, "Enhanced emission from Si-based light emitting diodes using surface plasmons," Appl. Phys. Lett. **88**(16), 161102 (2006).
20. H. R. Stuart and D. G. Hall, "Island size effects in nanoparticle enhanced photo- detectors," Appl. Phys. Lett. **73**(26), 3815–3817 (1998).
21. N. C. Das, "Tunable infrared plasmonic absorption by metallic nanoparticles," J. Appl. Phys. **110**(4), 046101 (2011).
22. U. Kreibig and M. Vollmer, *Optical Properties of Metal Clusters* (Springer, 1995).
23. F. J. Beck, A. Polman, and K. R. Catchpole, "Tunable light trapping for solar cells using localized surface plasmons," J. Appl. Phys. **105**(11), 114310 (2009).
24. R. D. Tilley and S. Saito, "Preparation of large scale monolayers of gold nanoparticles on modified silicon substrates using a controlled pulling method," Langmuir **19**(12), 5115–5120 (2003).
25. T.-S. Yoon, J. Oh, S.-H. Park, V. Kim, B. G. Jung, S.-H. Min, J. Park, T. Hyeon, and K.-B. Kim, "Single and multiple-step dip coating of colloidal maghemite (γ-Fe_2O_3) nanoparticles onto Si, Si_3N_4, and SiO_2 substrates," Adv. Funct. Mater. **14**(11), 1062–1068 (2004).
26. X.-H. Li, R. Song, Y.-K. Ee, P. Kumnorkaew, J. F. Gilchrist, and N. Tansu, "Light extraction efficiency and radiation patterns of III-nitride light-emitting diodes with colloidal microlens arrays with various aspect ratios," IEEE Photon. J. **3**(3), 489–499 (2011).
27. Y.-K. Ee, P. Kumnorkaew, R. A. Arif, H. Tong, H. Zhao, J. F. Gilchrist, and N. Tansu, "Optimization of light extraction efficiency of III-nitride LEDs with self-assembled colloidal-based microlenses," IEEE J. Sel. Top. Quantum Electron. **15**(4), 1218–1225 (2009).
28. P. Kumnorkaew, Y.-K. Ee, N. Tansu, and J. F. Gilchrist, "Investigation of the deposition of microsphere monolayers for fabrication of microlens arrays," Langmuir **24**(21), 12150–12157 (2008).
29. M.-A. Tsai, P.-C. Tseng, H.-C. Chen, H.-C. Kuo, and P. Yu, "Enhanced conversion efficiency of a crystalline silicon solar cell with frustum nanorod arrays," Opt. Express **19**(S1), A28–A34 (2011).
30. H.-C. Chen, C.-C. Lin, H.-W. Han, Y.-L. Tsai, C.-H. Chang, H.-W. Wang, M.-A. Tsai, H. C. Kuo, and P. Yu, "Enhanced efficiency for c-Si solar cell with nanopillar array via quantum dots layers," Opt. Express **19**(S5), A1141–A1147 (2011).
31. K. R. Catchpole and A. Polman, "Design principles for particle plasmon enhanced solar cells," Appl. Phys. Lett. **93**(19), 191113 (2008).
32. T. J. Kippenberg, A. L. Tchebotareva, J. Kalkman, A. Polman, and K. J. Vahala, "Purcell-factor-enhanced scattering from Si nanocrystals in an optical microcavity," Phys. Rev. Lett. **103**(2), 027406 (2009).
33. J. N. Munday, D. M. Callahan, C. Chen, and H. A. Atwater, "Three efficiency benefits from thin film plasmonic solar cells," in *Proceedings of Photovoltaic Specialists conference, 37th IEEE PVSC*, June 19–24 (Settle, Washington, 2011), # 279.
34. V. E. Ferry, J. N. Munday, and H. A. Atwater, "Design considerations for plasmonic photovoltaics," Adv. Mater. (Deerfield Beach Fla.) **22**(43), 4794–4808 (2010).
35. G. Bachelier, I. Russier-Antoine, E. Benichou, C. Jonin, N. Del Fatti, F. Vallée, and P. F. Brevet, "Fano profiles induced by near-field coupling in heterogeneous dimers of gold and silver nanoparticles," Phys. Rev. Lett. **101**(19), 197401 (2008).
36. Y. A. Akimov, K. Ostrikov, and E. P. Li, "Surface plasmon enhancement of optical absorption in thin-film silicon solar cells," Plasmonics **4**(2), 107–113 (2009).
37. M. A. Greenwood, "Photocurrent altered with nanoparticles," Photon. Spectra **106**, (2008), http://www.photonics.com/Article.aspx?AID=32563.

#160131 - $15.00 USD Received 16 Dec 2011; revised 13 Jan 2012; accepted 13 Jan 2012; published 20 Jan 2012

1. Introduction

Multicrystalline silicon (mc-Si) solar cells represent the mainstream products that have dominated the photovoltaic market since 1999 when they overtook the leading position of single-crystalline silicon (sc-Si) solar cells [1]. However, industrially available mc-Si solar cells exhibit a lower efficiency than their counterpart sc-Si solar cells due to loss mechanisms, namely, the optical, resistive and recombination losses. The sc-Si cells with pyramid texturing on the front have low optical losses. By contrast, the optical losses account for a 7% efficiency loss in commercial mc-Si solar cells [2], which include the front surface reflection (from screen-printed metal fingers and the imperfection of antireflection coating (ARC)), the absorption by the ARC and the back surface reflector, and the escape of long wavelength light through the front surface (imperfect light-trapping). The high optical losses are mostly a result of the fact that it is difficult to achieve effective textures on the mc-Si substrates due to their random grain orientations. Essentially, light-trapping in the near-infrared (NIR) is challenging with conventional surface texturing approaches, since the feature size of the texturing should be comparable to the wavelength of interest in order to scatter the light effectively [3]. To optimize the cell performance, light-trapping should be maximized for spectral regions where Si is poorly absorbing (near the band edge of the Si). Moreover, further enhancement in efficiency of mc-Si solar cells without overly increasing costs is of great interest for the next generation high-efficiency and low-cost solar cells and to retain their leading position in the marketplace.

Plasmonic nanoparticles (NPs) induced scattering as an emerging strategy offers a unique way to enhance light-trapping in solar cells [4–12]. To date, investigation of plasmonic NPs in mc-Si solar cells and demonstration of meaningful efficiency enhancement have not yet been reported although it is of paramount significance to the solar cell research and the photovoltaic industry.

In this paper, through the integration of size-optimized Au NPs into mc-Si solar cells, we show that the light absorption in the active layer of solar cells and thus the photocurrent as well as the external quantum efficiency (EQE) are consistently improved at longer wavelengths, while maintaining almost unchanged below the plasmon resonance wavelength. Consequently, the energy conversion efficiency is increased from 14.9% to 15.2% for solar cells incorporated 61 nm Au NPs. Unlike the samples in most plasmonic solar cell studies [6,8,11,12], where planar solar cells were investigated, we target the industrially available textured mc-Si solar cells already in production, which are more relevant and significant to the photovoltaic industry, to conduct our plasmonic NP investigation. Furthermore, a low-cost and facile dip coating method, which is mostly preferred by the photovoltaic industry for scaling-up production, has been implemented to integrate the size-tailored Au NPs with solar cells. This study shows the suitability of plasmonic Au NPs to enhance the light absorption and the efficiency of optically thick and industrial mc-Si solar cells.

2. Materials and experimental methods

2.1. Materials

Hydrogen tetrachloroaurate trihydrate ($HAuCl_4 \cdot 3H_2O$), sodium citrate and hydroxyamine were all purchased from Sigma-Aldrich. The as-received chemicals were used without any further purification and first distilled water was used for all solution preparation throughout all the experiments. All the glassware was scrupulously cleaned by soaking in aqua regia solution, which is especially crucial to ensure the absence of new particle nucleation (small particles).

#160131 - $15.00 USD Received 16 Dec 2011; revised 13 Jan 2012; accepted 13 Jan 2012; published 20 Jan 2012

2.2. Synthesis and characterization of Au NPs

2.2.1. Preparation of initial Au seeds

The Au seeds were synthesized according to Frens' method [13]. Briefly, an aqueous solution of 500 ml of 1 mM M $HAuCl_4$ was heated to boiling with stirring; then 50 ml 1% (wt/v) aqueous sodium citrate was added all at once. The colour of the mixed solution changed from yellow to wine red in several minutes, indicating the formation of Au NPs. The boiling and stirring were continued for 15 min. Then the heat source was removed and the stirring was continued for additional 15 min. The seed solution was cooled to the room temperature and used directly for further experiments. This method produced Au NPs with a mean diameter of 14.7 ± 1.56 nm according to the SEM and TEM images. The concentration of the Au seeds was estimated as ~1.6×10^{12} particles/ml. This initial Au seed batch was labelled as colloid "A".

2.2.2. Growth of Au NPs

A series of colloidal Au NPs with diameters in the range of 20 – 150 nm were prepared through the iterative seeding process with some modifications [14] by using HN_2OH as a reducing agent. Six subsequent Au colloids were prepared by taking six 300 ml conical flasks (labelled from "B" to "G"), hydroxylamine as reducing agent [0.375 – 1.25 ml] (labelled as *I*) was mixed with deionized water (50 – 135 ml) (labelled as *II*), then colloidal solution [15 – 55 ml] (labelled as *III*) was added and finally 1% hydrogen tetrachloroaurate [$HAuCl_4$, 1ml] (labelled as *IV*] was added under vigorous stirring at the room temperature. Addition of each reagent to the flask was conducted under vigorous stirring for 2 min. To prepare the colloid "C" with a specific particle size, colloid "B" was used as the seed; and to prepare colloid "D", colloid "C" was used as the seed and so on. With the above recipes, the calculated diameters of the resulting Au particles were 18, 32, 41, 56, 110 and 149 nm for B to G, respectively. Usually, Au colloids prepared by this method were stable for months under the proper storing conditions. Sedimentation was occasionally found, especially in the samples with larger particles, while the precipitate could be easily redispersed with a gentle shake; and the mean diameters of the Au NPs could be well preserved.

2.2.3. Characterization of colloidal Au NPs

The ultraviolet–visible-near infrared (UV-VIS-NIR) absorption spectra of Au colloidal solutions were measured with a spectrophotometer (Perkin Elmer, Lambda 1050), by using a quartz cuvette with a 10 mm optical path in the wavelength range from 300 to 1100 nm (DI water as a reference). Scanning electron microscope (SEM, FEI Helios NanoLab 600i equipped with an energy dispersive X-ray (EDX) unit) and transmission electron microscopic (TEM, FEI Tecnai F20) images were used to characterize the morphology of the Au NPs. The Au colloid was dripped onto the Si substrate and carbon-coated copper grid and air-dried at the room temperature for SEM and TEM imaging, respectively. The mean diameter and size distribution were measured from several SEM images by counting more than 100 NPs.

2.3. Integration of Au NPs with Si solar cells

Fifteen mc-Si solar cells with initial efficiencies of around 15% were selected, which represent the mainstream products from the photovoltaic industry. Before dipping, solar cells were washed with ethanol and dried by N_2 gas. Au NPs of size ranging from 50 to 150 nm were synthesized [4] and integrated onto the front surface of these solar cells by using a programmable dip coater (KSV company, model: DS). To integrate the Au NPs with the solar cells, the solar cells were mounted on a sample holder, vertically dipped into the colloidal Au solution, immersed for 4 min, and pulled out of the solution with a velocity of 30 mm/min, and then were left clamped on the sample holder till being dried in air at the room temperature. The pulling speed has been studied for 1, 5, 10, 30 and 50 mm/min and the

#160131 - $15.00 USD Received 16 Dec 2011; revised 13 Jan 2012; accepted 13 Jan 2012; published 20 Jan 2012

immersion time in the range from 2 to 10 min. It was found the speed of 30 mm/min and the immersion time of 4 min gave the relatively homogeneous distribution and the required surface coverage of about 12%.

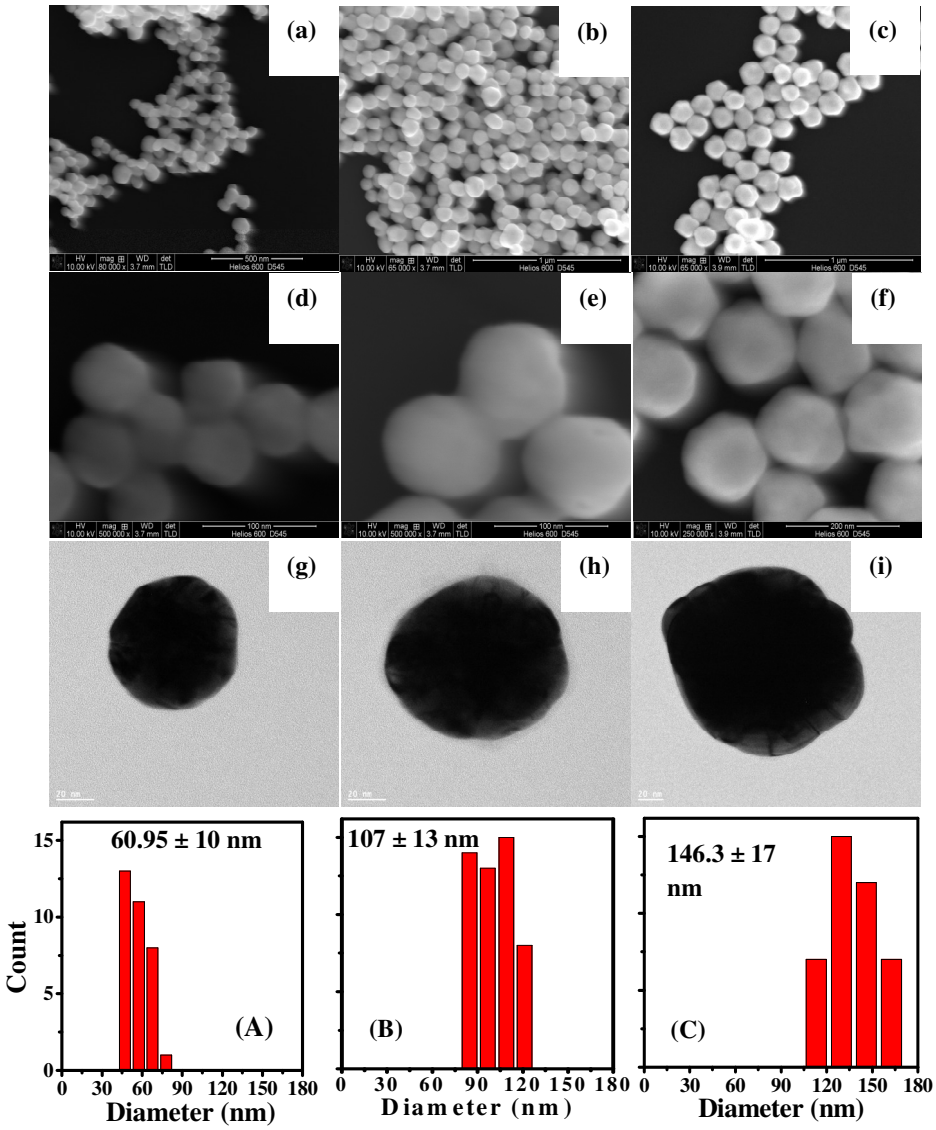

Fig. 1. FE-SEM micrographs for Au colloidal NPs of 61, 107 and 146 nm diameters, respectively at different magnifications {(a, d), (b, e), (c, f)}. High resolution TEM images of Au NPs of the above diameters (g, h, i), and histograms of particle size distributions for particle sizes of 61, 107 and 146 nm (A, B, C).

Commercial textured mc-Si solar cells (Suntech Power Holdings Co., Ltd.) with metal contacts and ARC were employed. The ARC is made of SiN_x of 90 nm in thickness and has a refractive index n of 2.01 at 632.8 nm, as determined by the ellipsometry measurements (J.A. Woollam M-2000XI). The integration of Au NPs on the top surface of all solar cells was conducted at the same conditions to ensure that the NP distributions are similar. For each particle size, 3 solar cells have been used, to avoid the reference cell uncertainty.

#160131 - $15.00 USD Received 16 Dec 2011; revised 13 Jan 2012; accepted 13 Jan 2012; published 20 Jan 2012

Au NP colloidal solutions of concentrations 1.28×10^{11}, 1.72×10^{10} and 7×10^{9} NPs/ml for sizes 61, 107 and 146 nm, respectively, were used. The Au NPs surface coverage on solar cells was estimated from the SEM micrographs by calculating the particle density and the geometrical area of the particles.

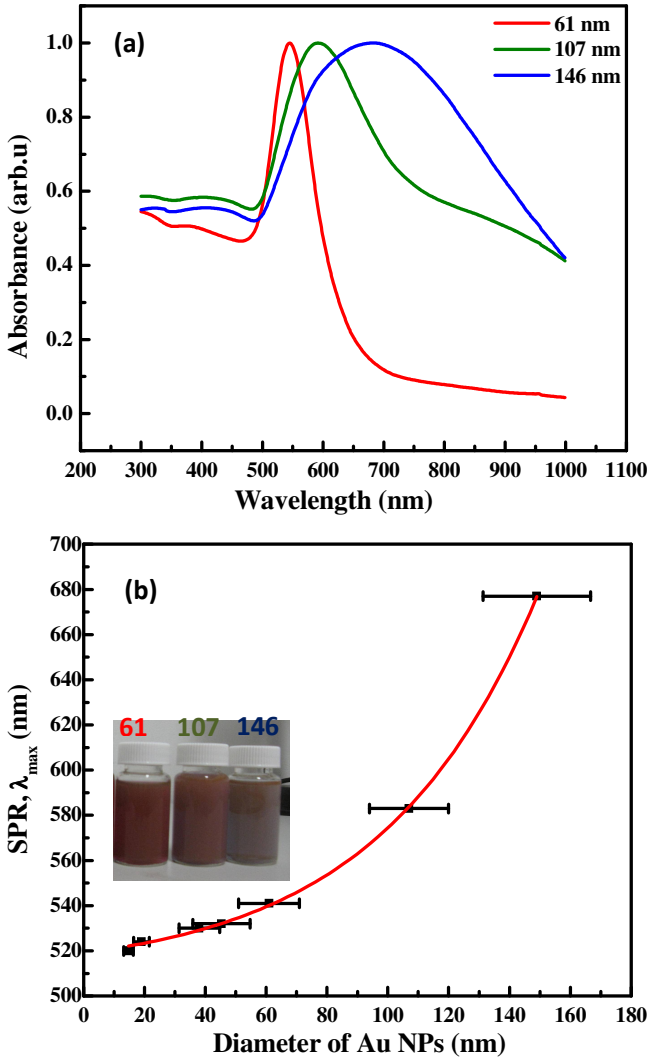

Fig. 2. UV-vis absorption spectra of 61, 107 and 146 nm diameter Au colloidal NPs suspended in an aqueous solution. Peaks corresponding to the excitation of SPR are evident in (a). The inset shows the photograph of the synthesized colloidal solutions of the NPs. The SPR peak position as a function of the Au particle diameter as estimated from the SEM images (b).

#160131 - $15.00 USD Received 16 Dec 2011; revised 13 Jan 2012; accepted 13 Jan 2012; published 20 Jan 2012

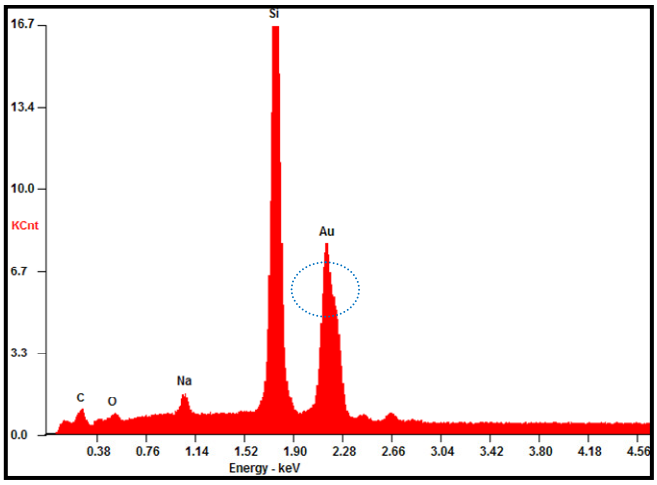

Fig. 3. EDX spectra of Au NPs deposited on the silicon substrate that supports the presence of Au peak. The trace from sodium detected in the spectra comes from the reactants.

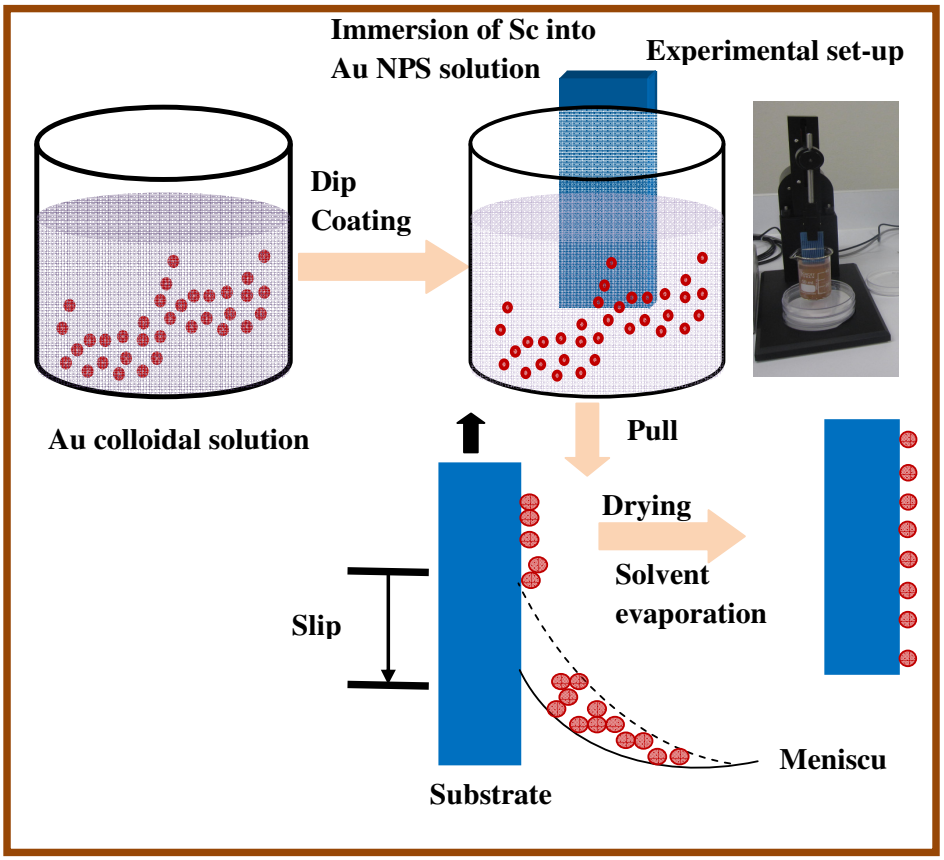

Fig. 4. A schematic diagram depicts the dip coating process to integrate Au NPs onto the top surface of Si solar cells. The real photograph of the experimental set-up is included.

2.4. Characterization of solar cells with and without Au NPs

All the solar cells with and without the Au NPs integrated onto the front surface were evaluated at 25°C based on the illuminated current density versus voltage (*J-V*)

#160131 - $15.00 USD Received 16 Dec 2011; revised 13 Jan 2012; accepted 13 Jan 2012; published 20 Jan 2012

characteristics, the EQE and the reflectance characterisation. The *J-V* curves were measured using a solar simulator (Oriel Sol 3A^{TM} class AAA, model 94023A) with a Keithley 2400 source meter under the Air Mass 1.5 Global (AM 1.5G) illumination condition (100 mW/cm^2) calibrated by a factory-calibrated Si module. The EQE was measured using the Bentham PVE300. The reflectance spectra of the samples were recorded by using an integrating sphere of the UV–VIS-NIR spectrophotometer (Perkin Elmer, Lambda 1050) for wavelengths ranging from 300 to 1200 nm.

All the measurements were conducted at different stages of sample processing. The effect of nanoparticles was determined by comparing each cell before and after nanoparticle integration. By this way, we ruled out the sample-to-sample uncertainty.

3. Results and discussion

3.1. Colloidal Au NPs

The resultant NPs present excellent monodispersity of the spherical particles without containing rod-shaped by-products as is showed from the SEM and TEM images (Fig. 1). Moreover, Au NPs of larger size ranging from approximately 20 to 150 nm with improved monodispersity (uniformity) have been acheived. By contrast, the original method [14] produces spherical NPs mixed with a distinct population (5-10%) of colloidal Au rods (141 ± 38 nm × 31 ± 4.6 nm). The fact that there is no rod-shaped by-product ensures that NPs of identical size are produced, offering a well-defined plasmonic response for our photovoltaic application. It is known that the optical properties (scattering, extinction and absorption) of nanoparticles are determined by both their size and shape and consequently their surface plasmon resonance [15]. Therefore, it is quite importance to apply the proper fabrication method to acheive tailored size and shape to support the desired resonances useful for solar cell performance enhancement.

It is worth noting that the solution-processable method to produce NPs is probably more preferable than the physical method that has mostly been adopted to apply metal NPs to semiconductor solar cells [3,6]. This is because the former method can be used to synthesize uniform NPs with a controlled particle size, whereas the synthesis of uniform-sized NPs and their size control are very difficult to achieve by the latter method. To use metal NPs for solar cell applications, the cost and effectiveness of the NP fabrication method become a significant issue. Obviously the colloidal chemical synthesis is a cheaper option with precise control over the size, shape and coverage of the NPs. In order to enhance light-trapping in silicon solar cells it is required that NPs to exhibit low absorption and large scattering cross-sections in the wavelength range of 300 – 1200 nm. NP absorption can be minimized by avoiding small particles. Since the enhancement of light absorption and hence the efficiency of light scattered into the Si active layer depend strongly on the particle size, Au NPs with different mean diameters of 61, 107 and 146 nm have been used.

Figure 1 shows the SEM (a – f) and TEM (g, h, i) images of the synthesized Au NPs with diameters of 61 (a, d, g), 107 (b, e, h) and 146 nm (c, f, i), respectively. The Au NPs were nearly spherical with uniform sizes and without any detectable by-products such as nanorods, triangles and small clusters. The measured mean diameters for Au NPs were 60.95 ± 10, 107 ± 13 and 146 ± 17.7 nm, as estimated from the FE-SEM micrographs and matched well with the calculated values (56, 110 and 149 nm). The statistical analysis of the particles for all sizes reveals a size distribution of the mean standard deviation ranging from 10 to 17 nm, indicating that NPs have a homogeneous size distribution as depicted in the histograms (Figs. 1a–1c). The surfaces are all smooth, evidently indicating that the Au NPs are single particles and not agglomerations of smaller units.

Absorption spectra measured for 61, 107 and 146 nm diameter Au colloidal NPs suspended in an aqueous solution confirm the existence of particle size dependent surface plasmon resonances (SPRs), as shown in Fig. 2a. Maxima in the absorption spectra are

#160131 - $15.00 USD Received 16 Dec 2011; revised 13 Jan 2012; accepted 13 Jan 2012; published 20 Jan 2012

evident at wavelengths corresponding to the surface plasmon excitations in the Au NPs. As expected, the peak red-shifts and broadens with increased particle diameter [15–21]. This trend can be explained as follows: for larger nanoparticles ($2R > 25$ nm) the extinction cross section is also dependent on higher-order multipole modes within the full Mie equation and the extinction spectrum is then also dominated by quadrupole and octopole absorption as well as scattering. These higher oscillation modes explicitly depend on the particle size and with increasing size the plasmon absorption maximum is shifted to longer wavelength and the bandwidth increases. The excitation of the higher-order modes is explained in terms of an inhomogeneous polarization of the nanoparticles by the electromagnetic field as the particle size becomes comparable to the wavelength of the exciting radiation. The broadening of the plasmon band is then usually ascribed to retardation effects [22]. In Fig. 2b the dependence of the plasmon resonance peak position is plotted versus the particle diameter. From this plot it can be seen that the peak position increases from 541 to 682 nm with increasing particle size from 61 to 146 nm. For mc-Si solar cells, which do not absorb well near the band-edge, plasmonic enhanced light-trapping in the long wavelength region is highly desirable [3,23].

To confirm the elemental composition and purity of Au NPs, EDX spectra have been measured for Au NPs deposited on silicon substrate, the presence of Au peak is evident in the spectra, as shown in Fig. 3.

3.2. Integration of Au NPs with Si solar cells

Optimizing the dipping conditions, including the pulling speed, immersion time and solution concentration, allows the control of the particle density. It was found that reducing the pulling speed increases the surface coverage. This is in good agreement with that previously mentioned [24]. Higher particle coverage of about 80% on Si substrate could also be acheived througth multiple-step dip coating [25]. Therefore, the dip coating method is fast, controllable and easy for the integration of NPs into solar cells. Moreover, one can form the particle layer with a high throughput without the waste of particles compared to other coating methods such as spin coating, which suffers from difficulties in delivering the exact amount of NPs onto the substrate, as well as difficulties in delivering particles onto a non-planar substrate. Other coating methods such as rapid convection deposition (RCD) and spin-cast have been reported to integrate colloidal NPs to light-emitting diodes (LED) [26–28] and solar cells [29,30]. Figure 4 presents a schematic diagram of the dip coating process to integrate Au NPs onto the top surface of mc-Si solar cells as well as a photograph of the real experimental set-up.

Figure 5 shows the Au NPs deposited on the front surface of mc-Si solar cells both for particle sizes 61 nm (a) and 107 nm (b, c). It is evident that the deposition of Au NPs by the dip coating method results in both isolated NPs and a few clustered NPs. These clustered NPs were probably formed when the nanospheres in the drying layer were attracted to each other by the capillary forces.

The area of clustered Au NPs was attributed to the interactions of several factors: solvent evaporation, capillary forces, particle-particle interactions, particle-substrate interactions, concentration gradient in the suspension, particle size, etc. Another possible reason for clustered area of Au NPs onto the solar cells is the surface texture of the front-surface of solar cell by which the particles are driven into texture via capillary force and form a multiple stacks. The uniformity of Au NPs onto solar cell can be improved by chemically modified surface of solar cell to change the surface polarities, through coating the solar cell with adsorption agent [25]. In addition, the following treatments can potentially improve the uniformity of the nanoparticle deposition: multiple-dipping process, thermal annealing of dip-coated solar cell before the next dipping without any chemical treatment of the solar cell, lowering the pulling speed, using higher boiling point solvent favoured the monolayer formation, diluting the particle concentration in solution, and pre-patterning of solar cell using glue.

#160131 - $15.00 USD Received 16 Dec 2011; revised 13 Jan 2012; accepted 13 Jan 2012; published 20 Jan 2012

The distribution of Au NPs on a large area of solar cell is shown in Fig. 5c. The surface coverage as deduced from the SEM micrographs was about 12%. Figure 5d shows the mc-Si photovoltaic device architecture incorporating the Au NPs on the front-surface of the device.

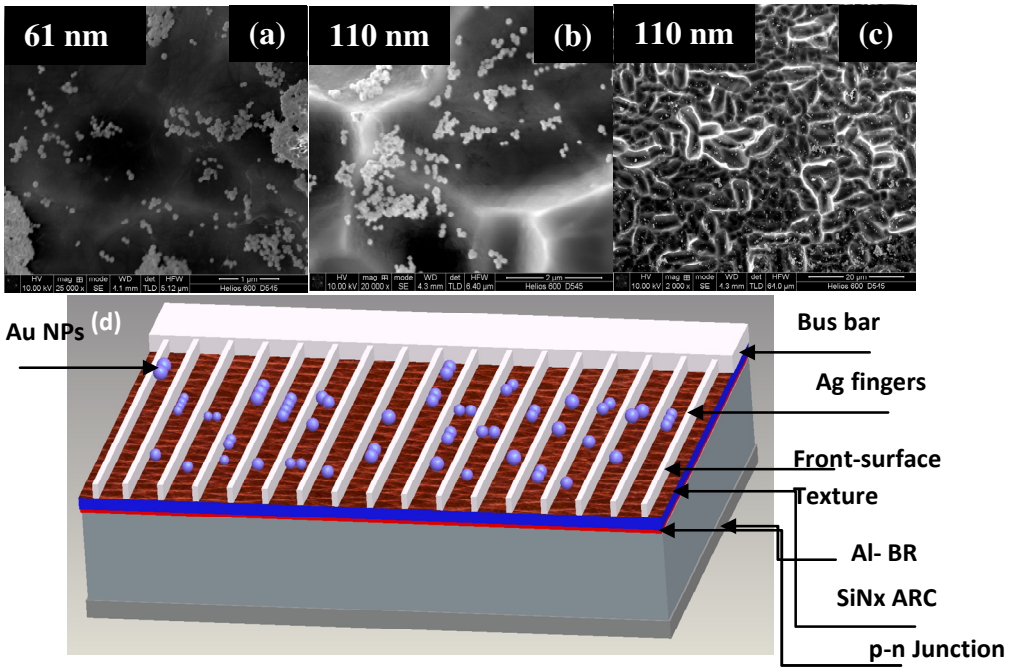

Fig. 5. FE-SEM micrographs of Au NPs of diameters 61 and 107 nm deposited on the top surface of mc-Si solar cells (a, b). The distribution of Au NPs on a large area of solar cells (c). The estimated surface coverage is about 12% from the SEM images. Mc-Si solar cell architecture incorporating Au NPs (d).

3.3. Photovoltaic characteristics of solar cells with and without Au NPs

3.3.1. Reflection spectra

The reflection spectrum of the mc-Si solar cell without NPs is shown in Fig. 6a. The reflectance ratios of cells integrated with Au NPs of mean diameters 61, 107 and 146 nm relative to the same cell prior to the integration are depicted in Fig. 6b. The reflectance was substantially reduced in the UV and NIR regions for the cells with Au NPs of mean diameter 61 nm. The reduction in reflectance was broad over the spectral range from 300 to 1200 nm with a sharp reduction peak by 25% centered at a wavelength of approximately 600 nm due to the SPR of the Au NPs, which exhibits λ_{SPR} close to 600 nm (as shown in Fig. 2a). On the other hand, for Au particles of sizes 107 and 146 nm, the reduction in reflectance is not broad over a large spectral range from 300 – 1200 nm. For Au NPs of diameter 107 nm, the reflectance reduced at longer wavelengths from 700 – 1200 nm, while at shorter wavelengths from 400 to 650 nm it slightly increases. It is also seen that the reflectance decreases at the wavelengths from 400 to 1000 nm but increases at $\lambda < 400$ nm and $\lambda > 1000$ nm for solar cells incorporated Au NPs of mean diameter 146 nm. It is expected that Au NPs of diameter 61 nm that reduce the cell reflectance across the entire solar spectrum should achieve the best enhancement in the solar cell performance as will be discussed in the EQE and *I-V* sections.

#160131 - $15.00 USD Received 16 Dec 2011; revised 13 Jan 2012; accepted 13 Jan 2012; published 20 Jan 2012

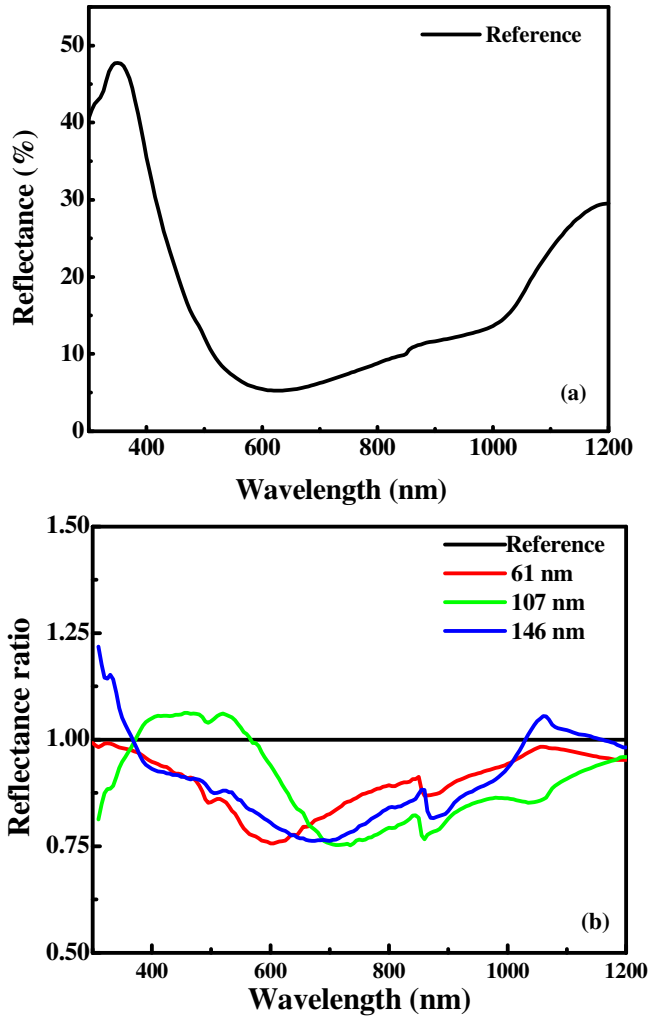

Fig. 6. Reflectance of mc-Si solar cells before integration with Au NPs (a). The reflectance ratio (normalized to the same cells without NPs) of cells integrated with Au NPs of diameters 61, 107 and 146 nm relative to the same cell prior to the integration (b). For Au NPs of size 61 nm, an improvement in reflectance of 7% is observed over wavelengths ranging from 300 to 1200 nm with a sharp reduction peaked at 600 nm (25%).

3.3.2. Quantum efficiency

The EQE of solar cells before integration of Au NPs as well as the EQE ratio of cells integrated with Au NPs of mean diameters 61, 107 and 146 nm relative to the same cell prior to integration are depicted in Figs. 7a and 7b, respectively. For cells with 61 nm Au NPs, it is evident from Fig. 7b that the EQE slightly reduces at $\lambda \leq 700$ nm, and significantly increases at longer wavelengths from $800 < \lambda \leq 1200$ nm. The EQE is enhanced by more than 11% at the wavelength of 1150 nm; this means the response of the solar cells should be improved at the NIR region.

#160131 - $15.00 USD Received 16 Dec 2011; revised 13 Jan 2012; accepted 13 Jan 2012; published 20 Jan 2012

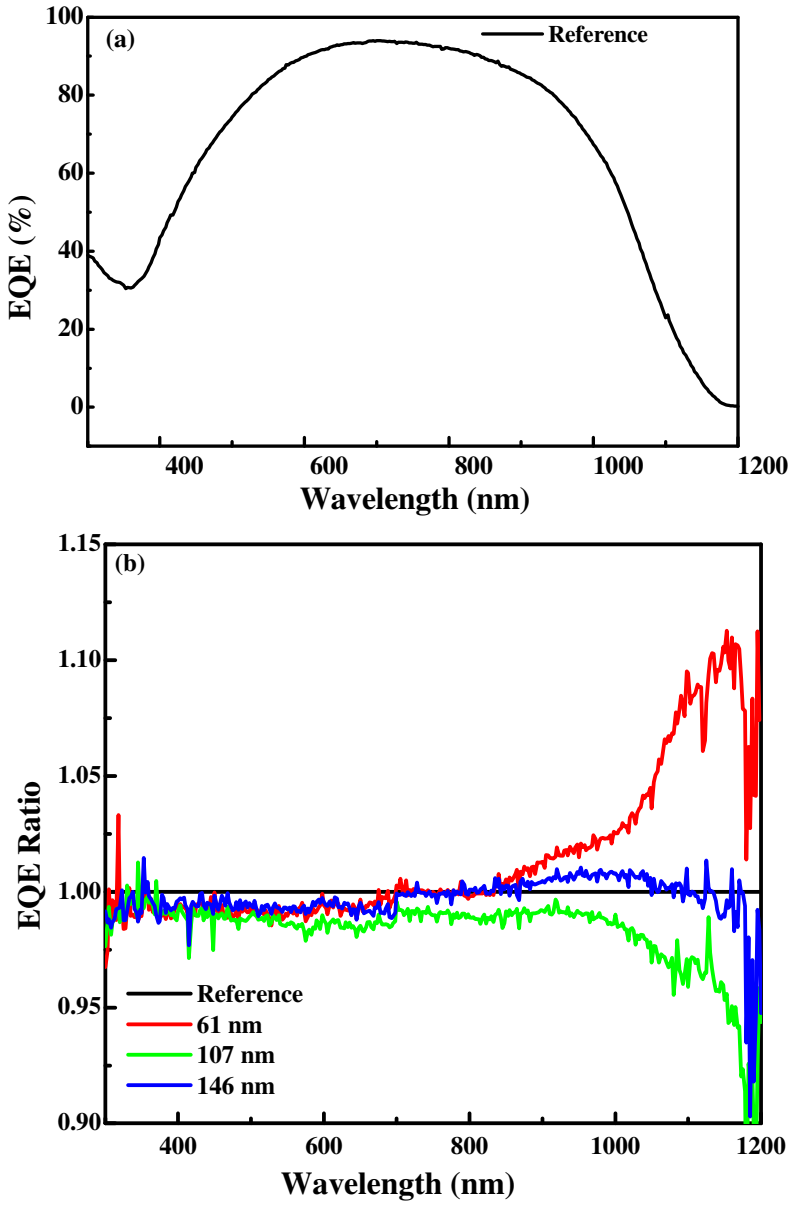

Fig. 7. EQE of solar cell prior to integration with NPs (a). EQE ratio (normalized to the same cells without NPs) of cells integrated with Au NPs of diameters 61, 107 and 146 nm relative to reference device prior to the Au NP integration is shown in (b). For Au NPs of 61 nm in diameter, it is evident that the EQE is enhanced by more than 11% at $\lambda = 1150$ nm and a broad enhancement over the spectral range from 800 to 1200 nm was achieved.

The reduction in the EQE response at the shorter wavelengths can be attributed to the phase shift, and the resulting destructive interference between the scattered light by the NPs and the light directly transmitted across the solar cell surface, specifically at wavelengths below the SPR of the NPs [9]. On the other hand, for longer wavelengths above the SPR, the EQE is significantly enhanced by the incorporation of the Au NPs of 61 nm in diameter. The mechanism behind this enhancement is due to the light-trapping provided by the scattering of

#160131 - $15.00 USD Received 16 Dec 2011; revised 13 Jan 2012; accepted 13 Jan 2012; published 20 Jan 2012

light by the dipolar resonance of the particles, which redirects the light preferentially forward into the solar cells [31,32]. This is consistent with the behaviour illustrated in Fig. 7b.

We note that the reflectance enhancement seen in Fig. 6b at short wavelengths ≤ 700 nm is not obvious in Fig. 7b; indeed EQE is reduced with all particle sizes for $\lambda \leq 700$ nm. This suggests that the reflectance enhancement at this wavelength is due to the absorption in the Au NPs, which does not contribute to the photocurrent generation. Since the reduction in reflectance is caused by a combination of forward-scattering and the absorption by the quadrupolar mode; the former increases the EQE, while the latter reduces it. This suggests that the EQE enhancement seen at the long wavelengths of 800 – 1200 nm is indeed caused by the light-trapping effects resulting from the scattering by the Au NPs. However, the reduction of reflectance for the solar cell with 107 nm NPs results in no increase in the EQE, while that with 146 nm Au NPs leads to a modest increase at the wavelength of 900 – 1100 nm. For the maximum enhancement in the solar cell performance we should balance between the photocurrent enhancements at the long wavelengths and the photocurrent suppression at the short wavelengths.

3.3.3. J-V characteristics

Table 1 presents the *I-V* parameters of mc-Si solar cells before and after the integration with Au NPs of diameters 61, 107 and 146 nm. It is evident that the highest enhancement in energy conversion efficiency was 1.97% with average enhancement of 1.2% for mc-Si cells integrated with Au NPs of mean diameter 61 nm. Since our target was to enhance the overall performance of mc-Si solar cell, the cell efficiency has been selected to monitor the performance of cell after integration with NPs. Moreover, both the short-circuit photocurrent density (J_{sc}) and the fill factor (*FF*) were enhanced by 0.93%. It is worth noting that the solar cells integrated with Au NPs of diameter 61 nm show an increases in all *I-V* parameters [J_{sc}, V_{oc}, *FF* and η] and also the enhancement in J_{sc} was confirmed by the EQE measurement (Fig. 7). It is interesting to note that the cell *FF* and V_{oc} are also improved upon integration of Au NPs on the surface of a solar cell. These results have also been reported for several photovoltaic cells [30,33,34]. The optimization of the particle size is of paramount importance because small particles show strong absorption and little scattering, hence reducing the amount of light transmitted into the solar cells. On the other hand, large particles have a strongly red-shifted resonance, resulting in a reduced transmittance in the shorter-wavelength range due to the Fano effect [35,36]. Therefore, properly designed metal NPs can strongly scatter NIR while maintaining minimum reduction in the visible range for high performance silicon solar cells [37]. Our results are in line with that reported by Schaadt et al. [4] who deposited spherical Au colloidal NPs of sizes 50, 80 and 100 nm on Si pn junction diode and observed maximum enhancement with Au particles of 80 nm in diameter.

Figure 8 presents the photocurrent density-voltage (*J-V*) characteristic of the solar cells at the maximum enhancement with 61 nm Au NPs. The performance of the cell without Au NPs is also included for comparison. J_{sc}, $V_{oc,}$ *FF* and η for the cell integrated with Au NPs are 35.7 mA/cm^2, 593.3 mV, 71.7%, 15.2% and for the reference cell are 35.4 mA/cm^2, 592.8 mV, 71.% and 14.9%, respectively. The energy conversion efficiency was improved from 14.9 to 15.2%; this means that it is enhanced by about 2%. All the I-V parameters of the mc-Si solar cells before and after the integration with Au NPs of diameters 61, 107 and 146 nm are summarized in Table 1.

#160131 - $15.00 USD Received 16 Dec 2011; revised 13 Jan 2012; accepted 13 Jan 2012; published 20 Jan 2012

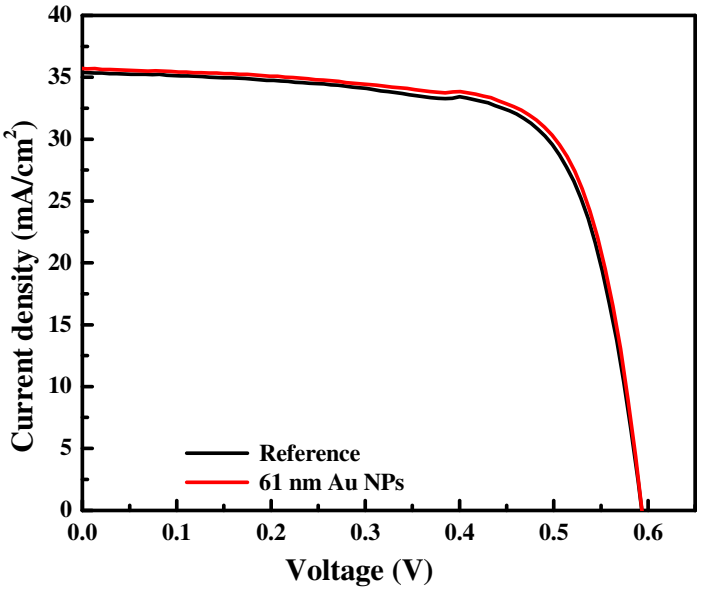

Fig. 8. *J-V* characteristic curve for solar cells before and after the integration with Au NPs of the mean diameter of 61 nm. All the photovoltaic characteristics were enhanced in this cell, namely, the overall energy conversion efficiency η (1.97%), J_{sc} (0.93%), *FF* (0.93%), and V_{oc} (0.096%).

Table 1. *I-V* Characteristic Parameters of the mc-Si Solar Cells Before and After Integration with Au NPs of Three Different Diameters

Solar Cells	V_{oc} (mV)	J_{sc} (mA-cm^{-2})	*FF* (%)	η (%)	η Relative Enhancement (%)
Without NPs	592.8	35.4	71.0	14.9	-
With 61 nm Au NPs	593.3	35.7	71.7	15.2	1.97
Without NPs	588.5	35.4	72.7	15.1	-
With 107 nm Au NPs	589.8	35.6	72.0	15.1	0.35
Without NPs	582.6	34. 4	73.8	14.8	-
With 146 nm Au NPs	584.0	34.6	73.6	14.9	0.82

***V_{oc}*: Open-circuit voltage, *J_{sc}*: Short-circuit current density, *FF*: fill factor, *η*: Energy conversion efficiency.**

4. Conclusions

We have demonstrated the fabrication and integration of colloidal Au NPs with industrially available textured mc-Si solar cells. A systematic study have been employed by selecting Au NPs ranging from 61 to 146 nm in diameter and integrating them into the mc-Si solar cells via dip coating, to fully optimize the SPR of Au NPs to enhance the solar cell performance. Integration of Au NPs of the optimized diameter of 61 nm onto the mc-Si solar cells has led to an increase of 0.93% in the short-circuit photocurrent density and 1.97% in the energy conversion efficiency compared to the textured reference solar cells without Au NPs. The EQE measurement has demonstrated a consistent increase in the photocurrent at the longer wavelengths ranging from 800 to 1200 nm. These enhancements are attributed to the enhanced light-trapping by the gold NPs in the Si photoactive layer. This study demonstrates a facile and cost-effective strategy based on the light-scattering by tailored plasmonic Au NPs to boost the conversion efficiency of textured mc-Si solar cells.

#160131 - $15.00 USD Received 16 Dec 2011; revised 13 Jan 2012; accepted 13 Jan 2012; published 20 Jan 2012

Acknowledgments

The authors acknowledge the financial support from the Victorian Government to establish the Victoria-Suntech Advanced Solar Facility (VSASF) under the Victoria Science Agenda (VSA) scheme. Yinan Zhang thanks Suntech Power Holdings Co., Ltd. for his PhD scholarship. Baohua Jia thanks the Victorian Government for the support through the Victorian Fellowship. The authors are grateful to CSG Pty. Ltd. for providing the access to QE equipment.

#160131 - $15.00 USD Received 16 Dec 2011; revised 13 Jan 2012; accepted 13 Jan 2012; published 20 Jan 2012